AD-A063 074 NAVAL RESEARCH LAB WASHINGTON D C F/G 20/5
MAGNETO-OPTIC MATERIALS FOR BIASING RING LASER GYROS.(U)
APR 78 J J KREBS, G A PRINZ

UNCLASSIFIED NRL-MR-3870 NL

1 OF 1

AD
A063 074

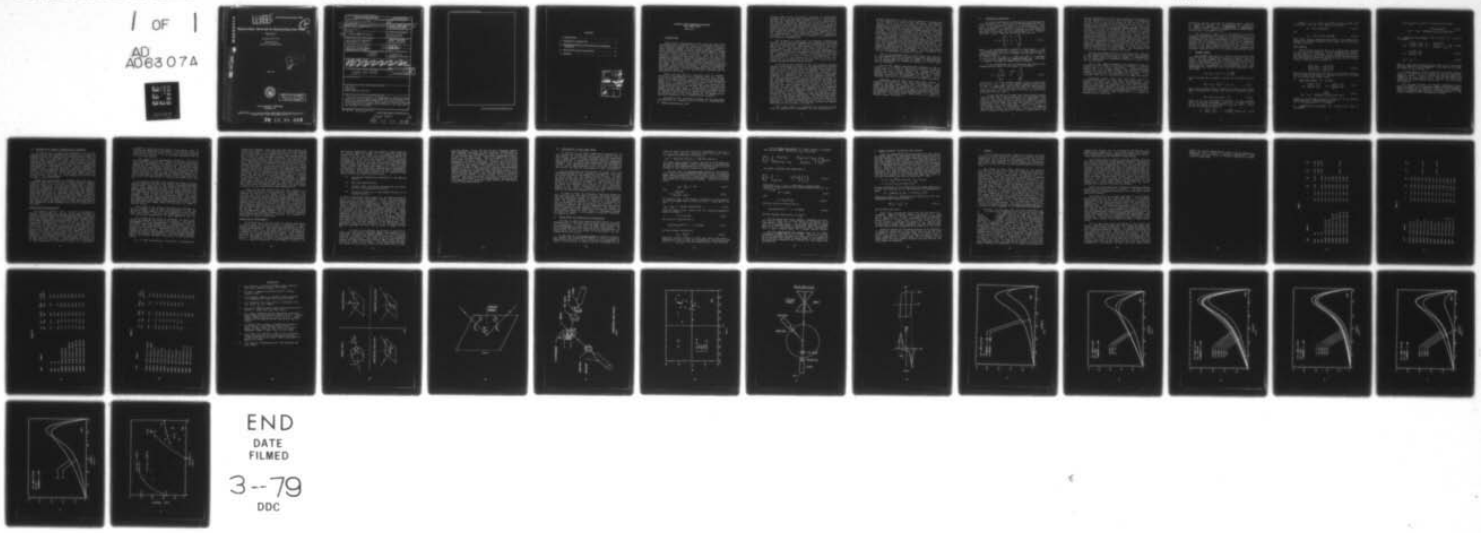

END
DATE
FILMED
3--79
DDC

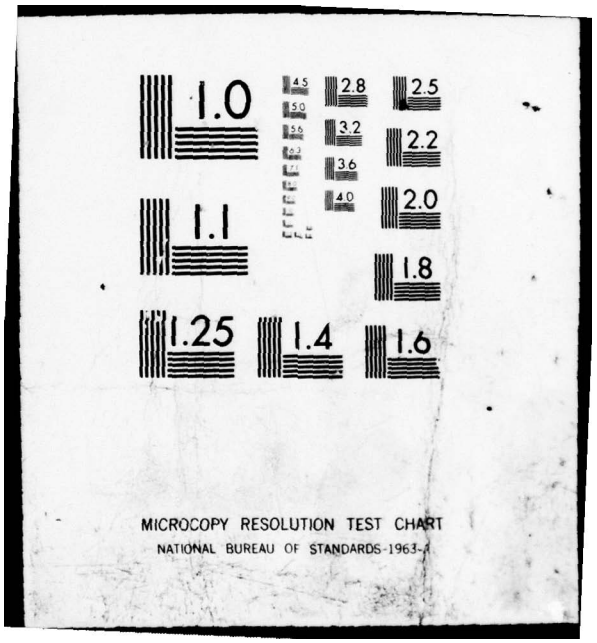
1.0
1.1
1.25
1.4
1.6
1.8
2.0
2.2
2.5
2.8
3.2
3.6
4.0
4.5
5.0
5.6
MICROCOPY RESOLUTION TEST CHART
NATIONAL BUREAU OF STANDARDS-1963-A

LEVEL II

NRL Memorandum Report 3870

Magneto-Optic Materials for Biasing Ring Laser Gyros

Report No. 1

J.J. Krebs and G.A. Prinz

Magnetism Branch
Electronics Technology Division

April 1978

NAVAL RESEARCH LABORATORY
Washington, D.C.

SECURITY CLASSIFICATION OF THIS PAGE (When Data Entered)

REPORT DOCUMENTATION PAGE

READ INSTRUCTIONS BEFORE COMPLETING FORM

1. REPORT NUMBER: NRL Memorandum Report 3870

2. GOVT ACCESSION NO.

3. RECIPIENT'S CATALOG NUMBER

4. TITLE (and Subtitle): MAGNETO-OPTIC MATERIALS FOR BIASING RING LASER GYROS, Report No. 1

5. TYPE OF REPORT & PERIOD COVERED: Interim report on a continuing problem.

6. PERFORMING ORG. REPORT NUMBER

7. AUTHOR(s): J.J. Krebs and G.A. Prinz

8. CONTRACT OR GRANT NUMBER(s): F21234

9. PERFORMING ORGANIZATION NAME AND ADDRESS
Naval Research Laboratory
Washington, DC 20375

10. PROGRAM ELEMENT, PROJECT, TASK AREA & WORK UNIT NUMBERS
62721N WF21-234
NRL Problem P02-09

11. CONTROLLING OFFICE NAME AND ADDRESS
Department of the Navy
Naval Air Systems Command
Washington, DC 20361

12. REPORT DATE
April 1978

13. NUMBER OF PAGES
40

14. MONITORING AGENCY NAME & ADDRESS (if different from Controlling Office)

15. SECURITY CLASS. (of this report)
Unclassified

15a. DECLASSIFICATION/DOWNGRADING SCHEDULE

16. DISTRIBUTION STATEMENT (of this Report)
Distribution limited to U.S. Government Agencies only; test and evaluation: April 1978. Other requests for this document must be referred to the Commanding Officer, Naval Research Laboratory, Washington, DC 20375.

DISTRIBUTION STATEMENT A
Approved for public release;
Distribution Unlimited

17. DISTRIBUTION STATEMENT (of the abstract entered in Block 20, if different from Report)
NRL-MR-3870

18. SUPPLEMENTARY NOTES

19. KEY WORDS (Continue on reverse side if necessary and identify by block number)
LPS Vol-4
Laser Gyros
Magneto-Optical Materials

20. ABSTRACT (Continue on reverse side if necessary and identify by block number)
A series of new materials, including magnetic glasses of Fe-Si and Fe-B in varying compositions, permalloys, Fe-overcoated permalloys and single element standards Fe, Ni, and Co have been fabricated and characterized. These results as well as an analysis of the application of magneto-optic materials to the laser gyro bias problems is presented.

DD FORM 1 JAN 73 1473 EDITION OF 1 NOV 65 IS OBSOLETE
S/N 0102-014-6601

SECURITY CLASSIFICATION OF THIS PAGE (When Data Entered)

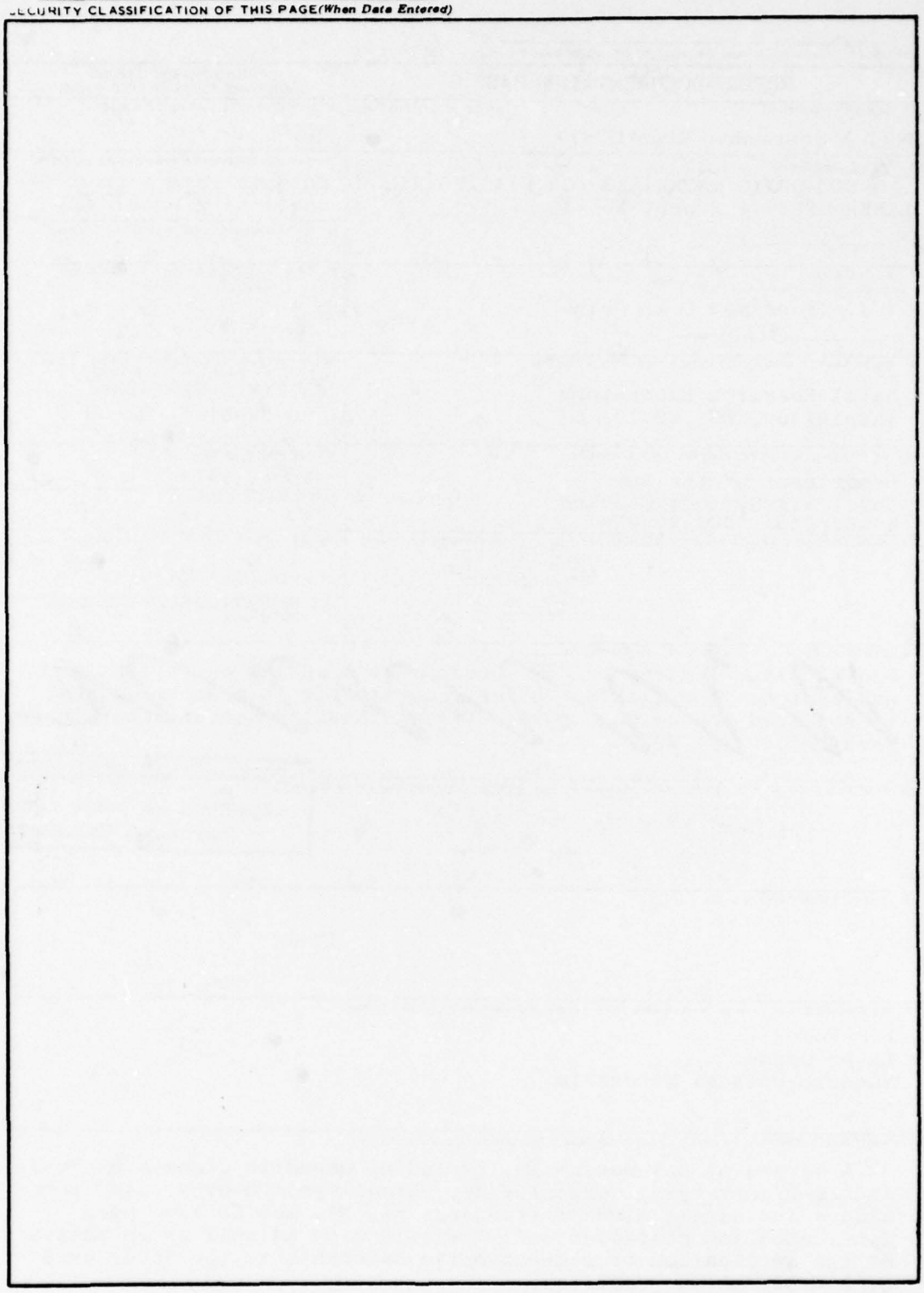

CONTENTS

I. INTRODUCTION 1

II. THEORETICAL BACKGROUND 4

III. PROPERTIES OF METALLIC MAGNETO-OPTIC MATERIALS .. MATERIALS 8

IV. APPLICATION TO RING LASER GYROS 13

V. SUMMARY 17

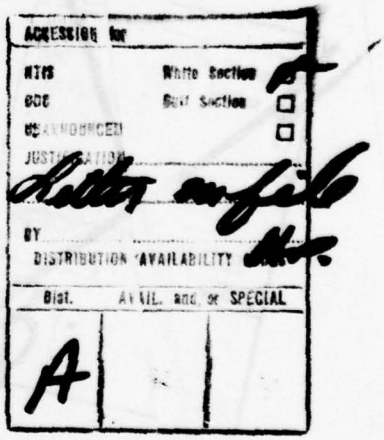

MAGNETO—OPTIC MATERIALS FOR BIASING RING LASER GYROS

Report No. 1

I INTRODUCTION

The earliest investigators of the ring laser gyro (RLG) recognized that in principle the most attractive solution to the fundamental problem of lock-in was to employ a magneto-optic biasing element. Unlike ordinary optical materials, these elements present an optical path which appears "longer" for light passing through it one way than it does for light passing in the opposite direction. When one of these elements is placed in the single cavity of a ring laser, the oppositely propagating beams find themselves in cavities of effectively different lengths, causing the single cavity of the ring laser to resonate at different frequencies for the two beams. Once these frequencies are sufficiently different, the beams "unlock" from one another. Because of fundamental physical laws which distinguish magnetism from electricity, only magneto-optic, and not electro-optic elements can be employed for this task.

There are two ways to construct such an element: either as a transmissive device (Faraday cell) or a reflective device (Kerr mirror). In either case one wants a high degree of differentiation between the two counter-propagating beams (i.e., a large magneto-optic effect) and as little attenuation as possible. Furthermore, one requires the device properties to be stable under the operating conditions imposed on the laser gyro. Unfortunately at present this elegant magneto-optic solution to the lock-in problem has not yet proved as satisfactory as "mechanical dithering". This is entirely due to the shortcomings in the properties of materials employed so far in magneto-optic elements.

Recognizing this continuing problem, and the long term desirability of a magneto-optics solution, NAVAIRSYSCOM

Ne . Manuscript submitted September 12, 1978.

through ADPO-35 has initiated a program to investigate systematically the problems of magneto-optic biasing and to develop new materials specifically for this application. The primary laboratory support for this task is to be provided by NRL which has the largest DoD effort in magnetic materials research. The program will pursue optimization of magneto-optic materials through an interactive procedure in which prototype elements prepared and characterized by NRL are tested by the participating industrial laboratories in RLG configurations. The materials preparation technology developed in this program will ultimately be transferred to the industrial laboratories.

The program is structured to achieve interaction between the materials development group (Magnetism Branch-NRL) and the participating industrial laboratories who will employ the magneto-optic (MO) elements in actual or simulated laser gyros. The program has three components: (1) Systematic analysis of the various M-O bias techniques to clarify the technological parameters governing each technique; (2) Preparation of a variety of promising materials and measurement of their relevant M-O parameters, (3) Transmission of the results of (1) and (2) to the RLG community and preparation of suitable M-O materials for system evaluation by RLG manufacturers.

Since the various industrial labs are currently pursuing several alternative solutions of the magneto-optic biasing problem, it is important that the program shall address as wide a variety of applications as possible. This will not only protect the proprietary industrial interests from exposure of information but will also ensure even-handed treatment in supporting the various industrial efforts. This can be made possible in a cost-effective manner if the characterizations of materials properties provided by NRL are made easily interpretable for all of the possible applications. To this end, NRL will provide an analysis of each of the useful magneto-optic effects which may be employed for gyro biasing. The analysis will be expressed in terms of the basic physical parameters of the material. The values of these parameters will be measured by NRL and provided for each sample. Using the analysis, each industrial user may then determine the expected performance in his own individual application. The theoretical background for this analysis is provided in the next Section of this report, and after presentation of the data for specific materials in Section III, the necessary formulas and sample calculations are provided in Section IV.

This first report is concerned with materials which might be employed as "switchable" (or AC) Kerr mirrors. A

typical application of such a mirror would be to replace one of the dielectric mirrors in the ring laser. The magnetization vector lies in the plane of the mirror and its polarity is alternatively switched back and forth. The magneto-optic biasing is then analogous to the rotational biasing obtained in the mechanical dither approach currently in use. In order to determine the usefulness of these materials, one must be provided with not only the optical and magneto-optical characteristics, but also with the static and dynamic magnetic properties. These latter properties determine for example, such things as the applied field which is required for switching and saturation. To this end ellipsometric determinations have been made of the real and imaginary indices of refraction, the real and imaginary magneto-optic coefficients at saturation and a dynamic magnetization (M) vs.magnetic field (H) loop (along with its derivative) for each sample. The techniques and results are described in Section III below.

All of the magnetic data in this report were obtained at room temperature and the magneto-optic data were obtained at the He-Ne laser wavelength of 6328Å. A supplementary set of magneto-optical parameters measured at 1.15μ will soon be available.

All of the samples measured were prepared at NRL as evaporated thin films on optically polished 1" diameter fused quartz (i.e.SiO_2) substrates. Evaporation was carried out using e-beam sources. The details of sample preparation have not been included in this report since material optimization is presumably not complete. It is intended that this information will be made available.

Subsequent reports shall deal with other classes of materials suitable for other gyro configurations. For example, the next report shall deal with materials which might be employed as "permanent" (or DC) Kerr mirrors. These mirrors would typically be used in a multi-oscillator configuration which employs circularly polarized light with the magnetization vector fixed perpendicular to the plane of the mirror. Following that, there will be a report on Faraday rotator materials.

II. THEORETICAL BACKGROUND

At visible and near-IR wavelengths the magneto-optical (M-O) properties of a material can be described entirely in terms of the dielectric tensor $\underline{\epsilon}$ of the material. This tensor is dependent, in general, on both the wavelength and the temperature. We restrict ourselves to cubic magnetic materials and assume the net magnetization M is directed along the z axis. Then the tensor has the form [1]

$$\underline{\epsilon} = \epsilon_o \begin{pmatrix} \kappa_1 & \kappa_2 & 0 \\ -\kappa_2 & \kappa_1 & 0 \\ 0 & 0 & \kappa_3 \end{pmatrix} \qquad \text{(II-1)}$$

where ϵ_o is the dielectric constant of free space, κ_1 and κ_3 are even functions of M, and κ_2 is an odd function of M. Since the effect of M on $\underline{\epsilon}$ is small, we can take κ_1 and κ_3 to have the form $\kappa_i = \kappa_i^0 (1 + \alpha_i M^2)$ and $\kappa_2 = \beta_2 \kappa_1^0 M$ with $\alpha_i M^2 << 1$, and $\beta_2 M << 1$. The α_i are in general all complex quantities. Note that κ_2 changes sign when the magnetization reverses.

It is traditional [2] to separate the optical and magneto-optical parts of the tensor $\underline{\epsilon}$ as follows:

$$\underline{\epsilon} = \epsilon_o \begin{pmatrix} N^2 & -iQN^2 & 0 \\ iQN^2 & N^2 & 0 \\ 0 & 0 & N^2 \end{pmatrix} \qquad \text{(II-2)}$$

where $N = n - ik$ is the complex optical index of refraction, $Q = Q_o e^{-i\phi} = Q_1 - iQ_2$ is the complex magneto-optical coefficient (or amplitude), and we have made the approximation $\kappa_3 \simeq \kappa_1 \simeq \kappa_1^o \equiv N^2$ in line with the results of Argyres[3]. Thus, we have $Q = i\beta_2 M$ so that Q (also Q_o, Q_1, Q_2) is proportional to M and $|Q| << 1$.

In what follows we consider only those magneto-optical effects which are linearly dependent on M and ignore those (such as the Voigt effect[2]) which are dependent on M^2. Only the linear effects will distinquish between two counter-propagating light beams and hence are useful in separating these beams in a ring laser gyro. These effects are 1) the Faraday effect in transmission and 2) the magneto-optical Kerr effect in reflection. The Kerr effect has three categories depending on relative orientations of the

typical application of such a mirror would be to replace one of the dielectric mirrors in the ring laser. The magnetization vector lies in the plane of the mirror and its polarity is alternatively switched back and forth. The magneto-optic biasing is then analogous to the rotational biasing obtained in the mechanical dither approach currently in use. In order to determine the usefulness of these materials, one must be provided with not only the optical and magneto-optical characteristics, but also with the static and dynamic magnetic properties. These latter properties determine for example, such things as the applied field which is required for switching and saturation. To this end ellipsometric determinations have been made of the real and imaginary indices of refraction, the real and imaginary magneto-optic coefficients at saturation and a dynamic magnetization (M) vs.magnetic field (H) loop (along with its derivative) for each sample. The techniques and results are described in Section III below.

All of the magnetic data in this report were obtained at room temperature and the magneto-optic data were obtained at the He-Ne laser wavelength of 6328Å. A supplementary set of magneto-optical parameters measured at 1.15μ will soon be available.

All of the samples measured were prepared at NRL as evaporated thin films on optically polished 1" diameter fused quartz (i.e.SiO_2) substrates. Evaporation was carried out using e-beam sources. The details of sample preparation have not been included in this report since material optimization is presumably not complete. It is intended that this information will be made available.

Subsequent reports shall deal with other classes of materials suitable for other gyro configurations. For example, the next report shall deal with materials which might be employed as "permanent" (or DC) Kerr mirrors. These mirrors would typically be used in a multi-oscillator configuration which employs circularly polarized light with the magnetization vector fixed perpendicular to the plane of the mirror. Following that, there will be a report on Faraday rotator materials.

reflecting surface, the plane of incidence and $\vec{M}$. They are a) polar: $\vec{M} \perp$ surface, b) longitudinal: $\vec{M} \parallel$ surface and $\vec{M} \parallel$ plane of incidence, and c) transverse (or equatorial): $\vec{M} \parallel$ surface but $\vec{M} \perp$ plane of incidence. The various configurations are illustrated in Fig. 1.

The dielectric tensor (II-2) and Maxwell's equations define the propagation of light in an M-O material. It is necessary also to treat the boundary conditions between the M-O material and its surroundings in order to completely specify the M-O effects on a light beam which propagates through or is reflected from the material. Freiser has given a clear and elegant treatment of the various M-O effects in his review article[1] and we merely summarize the relevant results here in a slightly generalized form.

A. Faraday Effect

We consider the case of a slab of M-O material with both $\vec{M}$ and the propagation direction normal to the slab faces. We also neglect the (relatively small) effect of surface reflections, and the interference effects which occur if the slab thickness ℓ is comparable to λ. The proper modes of propagation in the M-O material under these conditions are right and left circularly polarized (RCP, LCP) light

$$(E_x, E_y) = E_o(1, \pm i) \begin{cases} + \text{ RCP} \\ - \text{ LCP} \end{cases}$$

with corresponding complex indices or refraction given by

$$N_{\pm}^2 = (n_{\pm} - ik_{\pm})^2 = \kappa_1 \pm i\kappa_2 \qquad \text{(II-3)}$$

The relative phase shift between the RCP and LCP beams after propagating through the slab is therefore given by

$$\Phi = (2\pi\ell/\lambda_o)\, \mathrm{Re}(N_+ - N_-) \qquad \text{(II-4)}$$

where λ_o is the wavelength in vacuum. If the incident beam is linearly polarized, there is a Faraday rotation θ_F of the plane of polarization with $\theta_F = \Phi/2$. There is also an induced ellipticity

$$\epsilon_F = \frac{|E_+| - |E_-|}{|E_+| + |E_-|} = -\tanh\left\{\frac{\pi\ell}{\lambda_o}\, \mathrm{Im}(N_+ - N_-)\right\} \qquad \text{(II-5)}$$

Since $\kappa_1 \pm i\kappa_2 = N^2(1 \pm Q)$ from (II-2), we have from (II-3) that $N_+ - N_- = QN$. Hence we can write

$$\Phi = (2\pi\ell/\lambda_o)\mathrm{Re}(QN) \qquad \text{(II-4')}$$

and

$$\epsilon_F = \tanh\{(\pi\ell/\lambda_o)\mathrm{Im}(QN)\} \qquad \text{(II-5')}$$

Note that, since Q reverses sign with M, the phase shift between two counter-propagating RCP beams also is given by (II-4) or (II-4').

Kerr Effects

Let $\vec{E}$ be the electric vector of a light beam incident on a plane surface (see Fig. 2) with components E_p parallel to the plane of incidence and E_s perpendicular to it. Likewise let $\vec{R}$ be the electric vector of the reflected beam. The relationship between $\vec{R}$ and $\vec{E}$ is given by the complex Fresnel coefficients r_{ij} defined by

$$\begin{pmatrix} R_p \\ R_s \end{pmatrix} = \begin{pmatrix} r_{pp} & r_{ps} \\ r_{sp} & r_{ss} \end{pmatrix} \begin{pmatrix} E_p \\ E_s \end{pmatrix} \qquad \text{(II-6)}$$

We now give expressions for the r_{ij} for a semi-infinite slab in terms of the angle of incidence φ (Fig. 2), N, and Q for the various Kerr effect cases.

B. Polar Kerr Effect, ($\vec{M} \perp$ surface)

$$r_{pp} = \frac{N\cos\varphi - n_a\gamma'}{N\cos\varphi + n_a\gamma'} \qquad r_{ss} = \frac{n_a\cos\varphi - N\gamma'}{n_a\cos\varphi + N\gamma'} \qquad \text{(II-7)}$$

$$r_{ps} = r_{sp} = \frac{-iQNn_a}{(N\cos\varphi + n_a\gamma')(n_a\cos\varphi + N\gamma')} \qquad \text{(II-8)}$$

where n_a is the real index of refraction of the ambient medium adjacent to the $M=0$ material and $\gamma' = [1-(n_a/N)^2\sin^2\varphi]^{1/2}$ is complex.

C. Longitudinal Kerr Effect, ($\vec{M} \parallel$ surface, $\vec{M} \parallel$ plane of incidence)

Here r_{pp} and r_{ss} again are given by (II-7) and

$$r_{ps} = - r_{sp} = \frac{-iQn_a^2 \sin\varphi\cos\varphi}{\gamma'(N\cos\varphi + n_a\gamma')(n_a\cos\varphi + N\gamma')} \qquad \text{(II-9)}$$

D. Tranverse Kerr Effect, ($\vec{M} \parallel$ surface, $\vec{M} \perp$ plane of incidence)

$$r_{pp} = \frac{N\cos\varphi - n_a\gamma'}{N\cos\varphi + n_a\gamma'} \left\{1 - \frac{iQn_a^2 \sin 2\varphi}{N^2\cos^2\varphi - n_a^2\gamma'^2}\right\} \qquad \text{(II-10)}$$

$$r_{ss} = \frac{n_a\cos\varphi - N\gamma'}{n_a\cos\varphi + N\gamma'} \qquad \text{(II-11)}$$

$$r_{ps} = r_{sp} = 0 \qquad \text{(II-12)}$$

Thus in this case symmetry allows the p and s polarized electric vectors to be eigenmodes. Also there is no linear M-O effect on E_s since $\vec{E}_s \parallel \vec{M}$.

In some cases it is more convenient to use the relative index of refraction N' ($\equiv N/n_a$) of the M-O material. Equations (II-7) - (II-12) can be cast in this form if we replace n_a by unity and N by N'. For most M-O metals and alloys N' is sufficiently large that $\gamma' = 1.0$ is a good approximation.

For the Kerr effects, the Fresnel coefficients given above are sufficient to analyze a beam of arbitrary polarization incident on an opaque M-O material at an arbitrary angle of incidence and, as such, are quite general as long as the direction of $\vec{M}$ is constrained as shown.

III PROPERTIES OF METALLIC MAGNETO-OPTIC MATERIALS

In this section we shall provide data on the optical, magneto-optical and magnetization properties of some new materials which give promise for use as AC Kerr mirrors to provide bias in a ring laser gyro. We have also included similar data obtained on a few standard materials for reference and comparison purposes. These reference samples were prepared at NRL using the same thin-film evaporation techniques (see Introduction) as were used to prepare the new materials. They thus provide a reference "bridge" to connect the data presented here with other data which may be found in the literature. These reference samples are Fe, Ni, and Co, as well as two of the well known permalloy compositions: $Ni_{0.75}Fe_{0.25}$ (low magnetostriction) and $Ni_{.68}Fe_{.32}$ (low anisotropy).

There are three groups of compounds for which data is presented. The first is a series of "open sandwich" compositions in which a thin Fe film is placed upon a thicker permalloy underlayer. The motivation behind this construction is to combine the desirable square loop magnetic switching properties of permalloy with the high magneto-optic performance of Fe. The last two groups fall within a relatively new class of compounds called magnetic glasses. These are amorphous alloys of magnetic metal atoms (in this case Fe) along with glass-former atoms (in this case B and Si). As will be seen, some of these also combine the high magneto-optic performance of Fe with desirable switching properties, which amorphous Fe films by themselves do not have.

Magneto-Optical Measurements

The optical indices n and k, as well as the magneto-optical coefficients Q_1 and Q_2 which were defined in Section II were measured by standard ellipsometric techniques using a Gaertner Model L119 ellipsometer which had been specially fitted with a 0.5 milliwatt He-Ne 6328Å source and an EG&G radiometer/photometer Model 450-1. The setup is illustrated schematically in Fig. 3. The applied magnetic field for the transverse Kerr effect measurements was provided by a small electromagnet specially designed to fit on the ellipsometer stage holding the samples snugly within its 1" gap. The pole faces were shaped to provide a magnetic field which was uniform over the region of the sample and oriented perpendicular to the optical plane of incidence. The maximum field available was 120 Oe and its polarity could be reversed. The measurement procedure was to take data for the field in both polarities and average it, thus cancelling out systematic errors. It is important,

in order to have meaningful values for Q_1 and Q_2, that the samples be magnetically saturated. The precise value of the applied field at which this occurs will be discussed later in this section. All of the data presented will be for saturated samples.

One aspect of the measurement presented a difficulty which demanded special care. Since all of these Fe-bearing alloys are susceptable to oxidation, the top surface, once exposed to air, acquires an oxide film. Unless one knows the thickness and optical constants of this film to some precision one cannot extract from the ellipsometric measurements accurate values for the optical constants of the underlying alloy. This problem is especially acute for n and k, although the Faraday effect of the iron-oxide film may itself be large enough to distort the values of Q_1 and Q_2.

In order to overcome this problem and obtain accurate optical constants for the alloy itself, the transverse Kerr measurements were made at the surface between the fused quartz (SiO_2) substrate and the alloy film. That is, the samples were viewed from the back. The only difficulty with this approach is that any polarization change occuring when the beam passed through the SiO_2/air interface had to be avoided. Since no polarization change occurs for normal incidence, a special SiO_2 isosceles prism was constructed and installed on the sample stage of the ellipsometer. Its two equal sides presented faces perpendicular to the incident and reflected laser beams, while its base held the sample in optical contact.

The values of the optical constants thus obtained are given in Tables I and II under the headings n, k, Q_1^T, and Q_2^T The "T" here refers to the values measured in the transverse Kerr effect. The real and imaginary parts of Q are also presented graphically for each sample in Fig. 4.

As a check on Q_1 and Q_2 so obtained, the polar Kerr effect was measured for some of the samples. The optical arrangement for those measurements is illustrated in Fig. 5. The sample mount was replaced with a beam-splitter (Al film on SiO_2). The incident beam was passed down the bore of a large electromagnet and reflected from the sample held between its pole pieces. The reflected beam passed back through the bore to the beam-splitter where it was reflected toward the analyzer and detector. This arrangement guarantees a true normal incidence measurement of the polar Kerr effect.

If, in these measurements, there were no differential

reflectivity between right and left hand polarization from either the sample or the beam-splitter, one could prepare the incident beam to be linearly polarized and its rotation upon reflection from the sample would simply be measured by the rotation of the analyzer necessary to achieve minimum signal at the detector. This is not the case, however, and the differential reflectivity results in a non-zero ellipticity. This effect is countered by preparing the beam with a compensating amount of ellipticity using the $\lambda/4$ plate and the polarizer. As one can see from the figure, except for effects from the beam-splitter this experiment has axial symmetry about the incident beam, and therefore unlike the transverse Kerr measurements described earlier only two quantities can be measured which depend upon the sample, namely the settings of the polarizer and analyzer. In order to calculate Q_1 and Q_2 it is therefore necessary to assume values for n and k. The values determined from the transverse Kerr measurements were used. The effects caused by the metallic beam-splitter were not important since again data were taken for both field polarities, and the changes introduced by the beam-splitter were cancelled out.

Since the Faraday effect from the SiO_2 substrate in high fields would not be negligible, the samples were measured on the front (or exposed) face. From Table I one can see that most of the values of Q_1^P and Q_2^P ("P" here standing for polar) agree within the experimental uncertainties of $\pm$ 0.001 with the transverse data, indicating little Faraday effect from an oxide surface coating. It should be noted that Ni required too large a field to be saturated in the transverse apparatus, but in the 22kOe field used in the polar configuration yielded the saturated values shown for Q_1^P and Q_2^P. The only other marked discrepancy occured for the "sandwich" sample NIFE04. This is believed to arise from optical interference effects in the thin Fe overlayer which depend upon the angle of incidence. This question is discussed in Section V following.

Magnetization Measurements

As pointed out in the Introduction, useful application of these films requires not only a knowledge of their optical properties, but also detailed information on their magnetization behavior. The ideal condition of operation of a magnetic mirror in a ring laser gyro is for the material to always be in a saturated magnetic state. This condition provides the highest immunity to applied field changes, while at the same time giving the largest magneto-optic effects. Furthermore, if there is large magnetic anisotropy (i.e., a specific direction in the sample in which it is

more easily magnetized), then the sample is least sensitive to external magnetic fields if it is saturated along the "easy" direction. Of course, if one intends to employ the mirror in an AC mode, the above ideal condition is not realized during the time the polarity is being reversed. Furthermore, just as in the case of the mechanically dithered gyro, during the period of reversal bias diminishes and one passes through the "dead zone". The amount of time spent in this zone, where the laser gyro is not unlocked, contributes to the random drift problem and is therefore to be minimized. Hence, considering all of these requirements, the materials of greatest interest for AC transverse Kerr effect mirrors are those materials which:

a) Are easily magnetically saturated in low applied fields;

b) Have high magnetization;

c) Exhibit large anisotropy constraining the moment to lie in the plane of the mirror;

d) Allow the polarity of the magnetization to be reversed quickly.

In order to determine these properties, two separate measurements of each sample were made. First, the saturation magnetization M_s was measured in large magnetic fields applied parallel and perpendicular to the plane of the film using a vibrating coil magnetometer. These data are contained in Table III . Second, a hysteresis loop of M vs H, was obtained, as well as its derivative (dM/dt) vs H using an apparatus of the type described by Copeland[4]. These loops were obtained in applied fields up to 70 Oe using Helmholtz coils driven sinusoidally at 100 Hz. They were recorded photographically with an oscilloscope camera. Representative curves are shown in Fig. 6. From these curves the apparent saturation magnetization M_s' (i.e. the magnetization at maximum magnetic field amplitude), the switching field H_s and the width of the switching region ΔH_s were obtained, and this data is given in Tables III and IV.

In order to calibrate the M axis in the M vs H data, the most easily saturated sample was assumed to be saturated. Choosing this sample (FEB02) to be the reference standard, its value of M_s' was fixed to agree with M_s obtained from the magnetometer. The value of M_s for the remaining samples was then obtained by scaling their signal per unit volume as compared with FEB02. The discrepancies between the values of M_s and M_s' found for the same material stem

from two causes. First, the size of the 1" diameter samples were somewhat oversized for the existing configuration of the vibrating coil magnetometer, resulting in the material at the outside edge of the films being inadequately represented in the measurement. This is probably the problem with those values in Table III where $M'_s > M_s$ since the permalloys are easily saturated. Second, the 70 Oe field available in the M' vs H apparatus was not always sufficient to saturate the sample. The results of this are found largely in Table IV where the Fe-Si series only approached saturation as the Si concentration increased. This is very useful information, since for laser gyro applications it is important that saturation, not only switching, be achieved in low applied fields. In this regard, the Fe-B series by contrast not only switched, but also saturated in low fields. Modification of the magnetometer and hysteresis loop apparatus will eliminate these sources of discrepancy in any future measurements.

IV. APPLICATION TO RING LASER GYROS

In Section II the basic theoretical expressions for the various M-O effects were given, and in Section III our measurements of the optical and magneto-optical parameters for a large number of easily switched magnetic alloy films were tabulated. As mentioned earlier, the four fundamental parameters n,k, Q_1 and Q_2 were determined by ellipsometric methods. The transverse Kerr effect was used for most of the Q_1 and Q_2 measurements since the same ellipsometer setup could be used for simultaneous n and k measurements.

We now show how one can derive the phase shift and transmission/reflectivity information needed for ring laser gyro applications of the magneto-optical effects. A figure of merit $(FM)_T$ for the transverse Kerr effect is then defined and we show how the figure of merit varies as a function of the angle of incidence φ. The effect of transparent SiO_2 overcoating on $(FM)_T$ is then calculated since we expect any magnetic alloy mirrors to use a dielectric stack on top. Curves showing how the overcoated $(FM)_T$ depends on the angle of incidence are then displayed for each of the materials measured in Section III.

In order to keep the discussion relatively simple we have covered only the cases involving semi-infinite media and have explicitly ignored the details of "thin" magnetic films and dielectric stacks on either side of the magnetic film. By suitably matching the indices of refraction and the thicknesses in the film and/or the stack(s) it is possible to improve some of the magneto-optical performance characteristics of such magnetic mirrors. For details on how to handle multilayer dielectric and magnetic stacks and interference effects in these films in a systematic manner we refer the reader to the papers of Hunt[5], Smith[6], and Tanaka et al[7].

A. Phase Shift and Reflectivity/Transmission

In order to apply any magneto-optical effect as a bias mechanism for a ring laser gyro one must have the following M-O information: 1) the relative phase shift between two counter-propagating beams with the same polarization, 2) the relative and absolute reflectivity (or transmission) for these beams, and 3) the change in polarization, if any, induced by the M-O effect.

In the case of the Faraday effect at normal incidence, the formulas and discussion of Section II give the relative phase shift (see (II-4')) and, since they are eigenmodes, no change in polarization of either a RCP or a LCP beam. It is

easy to show that the relative transmission $|E_+/E_-|^2 = 1 + 4\epsilon_F$ (see (II-5')) using the fact that $\epsilon_F << 1$, while the absolute transmission is given by

$$|E_{\pm}|^2 = |E_{\pm}^o|^2 \exp(-4\pi \ell k_{\pm}/\lambda_o) \simeq |E_{\pm}^o|^2 \exp(-4\pi \ell k/\lambda_o).$$

For other than normal incidence the RCP and LCP modes mix because of differential p and s reflectivity at the surfaces. We ignore this complication for the present since it is not germane to the principal results of this report.

We now treat the transverse Kerr effect in more detail. This case has the advantage that the p and s polarized beams remain eigenmodes for an arbitrary angle of incidence and furthermore only the p beam shows a linear M-O effect. Thus there are no polarization changes. From (II-10) we can write

$$r_{pp} = r_{pp}^o (1 + AQ) \qquad \text{(IV-1)}$$

with

$$A = \frac{-in_a^2 \sin 2\varphi}{N^2 \cos^2\varphi - n_a^2 \gamma'^2} \qquad \text{(IV-2)}$$

The quantity r_{pp}^o is the Fresnel coefficient in the absence of any M-O effect and is given by (II-7). Using $AQ << 1$, we get

$$r_{pp} = r_{pp}^o \{1 + \mathrm{Re}(AQ)\} \exp\{i\,\mathrm{Im}(AQ)\} \qquad \text{(IV-3)}$$

Thus the phase shift between the two counter-propagating beams is given by

$$\Phi = 2\ \mathrm{Im}\ (AQ), \qquad \text{(IV-4)}$$

The relative reflectivity is

$$|E_p(\mathrm{cw})/E_p(\mathrm{ccw})|^2 = 1 + 4\ \mathrm{Re}(AQ), \qquad \text{(IV-5)}$$

and the average reflectivity

$$R_p = |r_{pp}^o|^2 . \qquad \text{(IV-6)}$$

Equations closely related to (IV-4) and (IV-5) were used to determine Q_1 and Q_2 from the ellipsometric measurements of Φ and $\delta\rho \equiv \delta\,|r_{pp}/r_{ss}|$ when the magnetization M was reversed.

For the polar Kerr effect it is more natural to consider RCP and LCP beams. Taking $E_{\pm} = E_p \pm iE_s$ we get

$$\begin{pmatrix} R_+ \\ R_- \end{pmatrix} = \begin{pmatrix} \frac{1}{2}(r_{pp}+r_{ss}) & \frac{1}{2}(r_{pp}-r_{ss})+ ir_{ps} \\ \frac{1}{2}(r_{pp}-r_{ss})- ir_{ps} & \frac{1}{2}(r_{pp}+r_{ss}) \end{pmatrix} \begin{pmatrix} E_+ \\ E_- \end{pmatrix} \quad \text{(IV-7)}$$

At normal incidence this simplifies to

$$\begin{pmatrix} R_+ \\ R_- \end{pmatrix} = \begin{pmatrix} 0 & r_{pp}+ir_{ps} \\ r_{pp}-ir_{ps} & 0 \end{pmatrix} \begin{pmatrix} E_+ \\ E_- \end{pmatrix} \quad \text{(IV-7')}$$

since then $r_{ss} = - r_{pp}$. Continuing to assume normal incidence we then get that the relative phase shift $\Phi = 2 \times \mathrm{Im}(ir_{ps}/r_{pp})$ or

$$\Phi = 2\ \mathrm{Im}(BQ) \quad \text{(IV-8)}$$

with

$$B = Nn_a/(N^2-n_a^2). \quad \text{(IV-9)}$$

Also the relative reflectivity is

$$|E_+(cw)/E_+(ccw)\ |^2 = 1 + 4\ \mathrm{Re}(BQ) \quad \text{(IV-10)}$$

and the average reflectivity is $|r^o_{pp}|^2$.

For the polar Kerr case, however, inspection of (IV-7) and (II-7) shows that if the angle of incidence $\varphi \neq 0$ (non-normal), then $r_{pp} \neq - r_{ss}$ so that RCP and LCP beams are not eigenmodes. Thus a circularly polarized incident beam will be elliptically polarized after reflection. This is not a magneto-optic but a purely optical effect.

For the longitudinal Kerr effect there are no simple eigenmodes except for $\varphi = 0$ or 90^o. These are trivial since the M-O effect vanishes for these φ's. As a result we do not discuss this effect in detail since it is inferior to the polar and transverse Kerr effects for ring laser gyro applications.

B. Figure of Merit (Transverse Kerr Effect)

Since the experimental results presented in this report are useful mainly for transverse Kerr RLG applications, we briefly discuss a suitable magneto-optical figure of merit for the transverse Kerr effect. One might be tempted to take the product of the phase shift and reflectivity $|r_{pp}|^2$ for counter-propagating p-polarized beams as the figure of merit. However, this ignores the fact that one will always have a dielectric mirror stack on top of the metallic mirror. Most of the reflected beam intensity will come from the stack, not from the metal. To evaluate the phase shift induced in the beam by M-O effects one must add vectorally the optical electric field reflected from the stack E_o and that reflected from the M-O mirror $E_m e^{i\alpha}$. Thus

$$E = E_o + E_m e^{i\alpha} \text{ and, since } E_m << E_o, \text{ we get}$$

$$E \simeq E_o \exp (iE_m \sin \alpha / E_o) \equiv E_o e^{i\beta}$$

We are interested in the differential M-O phase shift $d\beta$ of E when one reverses M (or the direction of propagation). Thus

$$d\beta = (\cos\alpha / E_o)\, E_m\, d\alpha = (\cos\alpha / E_o)\, E_m\, \Phi .$$

Since $E_m \propto |r^o_{pp}|$, a reasonable RLG definition for the transverse Kerr figure of merit is

$$(FM)_T = |r_{pp}{}^o|\ \Phi \qquad \text{(IV-11)}$$

and we adopt that here.

Both $|r^o_{pp}|$ and Φ are functions of the angle of incidence and the ambient index of refraction n_a. (See (II-7) and (IV-4).) In Fig. 7 we show plots of $^a(FM)_T$ vs φ for Fe based on the N and Q measurements in Section III. Plots for $n_a = 1$ (air) and $n_a = 1.457$ (SiO_2 at 0.633 μ) are shown to illustrate the effect of n_a. We see that increasing n_a makes $(FM)_T$ increase for all angles. This is the result of the corresponding increase of A in (IV-2).

Since we expect all M-O metal mirrors to be covered by a dielectric stack with a SiO_2 first layer we use the data of Tables I and II to generate $(FM)_T$ vs φ plots for $n_a = 1.457$. The results are shown in Figs. 8,9,10,11, and 12 where materials of a single class are all plotted in the same figure and each figure contains the pure Fe plot for the purpose of reference.

V. SUMMARY

In this section we shall compare the results obtained from the various materials which were studied and make suggestions as to which of them show promise for further development and which should be abandoned. In addition we shall make some comments on sample preparation techniques and what effect they have on the observed materials properties.

The figure of merit $(FM)_T$ described in the previous section will be used as the basis for comparing the performance of these materials. In order to make the comparison meaningful, we shall approximate the application in a typical ring laser gyro having an equilateral triangular configuration. In this case the angle of incidence at the top of the dielectric stack on a mirror is 30^o, but the angle of incidence at the metal surface is decreased to less than this by refraction. For our purposes we shall consider a single layer of SiO_2, which reduces the angle of incidence from 30^o to 20^o. One can then extract from Figs. 8, 9,10,11, and 12 the value of $(FM)_T$ at 20^o for each compound, and display them as a function of composition as shown in Fig. 13. Inspection of this figure shows that the data do not always vary smoothly as a function of composition. This is largely due to the extremely sensitive dependence of $(FM)_T$ on the components of Q. Even though we believe that data to be accurate to $\pm$ 0.001, in many cases this uncertainty can be significant. We have therefore taken the liberty of drawing a smooth curve merely to guide the eye to indicate our best judgement of the compositional dependence.

From Fig. 13 one sees that the peak performers are the well-known Ni-Fe compounds which are collectively known as Permalloys. The application of pure Fe faces 125Å thick had little effect, and faces 250Å thick actually degraded the performance. At first this may seem surprising since the magneto-optic coefficient |Q| was significantly enhanced by Fe facing, as shown in Fig. 4. This enhancement was accompanied by a decrease in reflectivity, causing an overall decrease in $(FM)_T$. The fact that the changes depend upon the thickness of the Fe faces is important. A careful study of thin Fe films prepared using the same evaporative techniques used here has shown [8] that the magneto-optic properties were dominated by interference effects in films up to ~ 800 Å thick for 6328Å radiation. In particular, significant enhancements in $(FM)_T^2$ were obtained for films 200Å to 500Å thick coated with glass of index $n_a = 1.52$. In view of this result it would seem that additional work on interference effects is justified. Before leaving the Permalloys, it is worth noting that the

compositions chosen, are not necessarily optimum for this magneto-optic application. The rising trend in performance with increasing Fe content suggests that additional compositions containing more Fe should be investigated.

The second group of samples contains examples from the new class of materials called magnetic glasses. Two families were studied containing glass formers Si and B respectively. The Si series was disappointing. Both |Q| and the optical constants changed slowly as the Si concentration was increased. The resulting materials all performed worse than pure Fe and therefore further work on the Si series does not appear worthwhile. The B series is much more promising, since in the range of B concentration of 50% to 15% the $(FM)_T$ increased monotonically to well above the value for pure Fe. The material with the lowest B concentration studied (i.e. 15%) approaches the performance of the permalloys. There seems little doubt that the region between 15% B and pure Fe should be studied.

There are three additional families of magnetic glasses, formed by alloying Fe with C, P, and S. In light of the Fe-B results it appears worthwhile to investigate these additional glasses.

The final point to be made from Fig. 13 is the observation that pure Co has a very good $(FM)_T$. Its principal shortcoming, as can be seen from Table III, is that it demands a rather high switching field and, perhaps more importantly, it switches slowly over a large range of applied field. Its switching properties are in fact much like that of pure Fe. It is known that alloying Co with Fe can improve the switching properties dramatically [9], but the magneto-optic properties of evaporated thin films of these alloys have not to our knowledge been determined. The alloys for which data is available have undesirably large anisotropy, so that even through they switch quickly in low fields, they require large applied fields to reach saturation.

All of the alloy films considered in this report are binary compositions formed from two e-beam sources, each providing an elemental component. For stationary substrates, this technique generally imposes a uniaxial anisotropy in the plane of the film. The easy axis lies in a plane perpendicular to the axis joining the two sources. The data provided in Tables III and IV were all measured for this easy axis. The use of mirrors made by this technique in an actual ring laser would require that this easy axis be aligned parallel to the plane of the ring for optimum performance. Ultimately, if these materials should prove

useful for mirror applications, they could be prepared by sputtering from a target of optimized composition. This technique can yield films of uniform composition without uniaxial anisotropy.

TABLE I

CODE	SAMPLE	n	k	Q_1^T	Q_2^T	Q_1^P	Q_2^P
FE01	FE	2.75	3.23	0.034	-0.000	0.030	-0.001
NI01	NI	1.80	3.24			0.006	-0.004
CO01	CO	2.25	3.64	0.026	-0.005	0.027	-0.007
NIFE06	NI-FE (0.75,0.25)	2.16	3.35	0.015	-0.011		
NIFE07	NI-FE (0.68,0.32)	2.23	3.42	0.018	-0.011		
NIFE02	NI-FE (0.8,0.2) 250A FE	2.64	2.95	0.035	-0.004		
NIFE03	NI-FE (0.8,0.2) 125A FE	2.64	3.11	0.035	-0.007		
NIFE04	NI-FE (0.68,0.32) 250A FE	3.10	3.52	0.043	-0.010	0.027	-0.021
NIFE08	NI-FE (0.68,0.32) 125A FE	2.52	3.08	0.032	-0.009		
NIFE09	NI-FE (0.75,0.25) 250A FE	3.06	3.39	0.038	-0.012		

TABLE II

CODE	SAMPLE	n	k	Q_1^T	Q_2^T	Q_1^P	Q_2^P
FESI01	FE-SI (0.9,0.1)	2.59	2.95	0.023	0.001		
FESI02	FE-SI (0.9,0.1)	2.60	2.96	0.029	0.002		
FESI03	FE-SI (0.85,0.15)	2.58	2.95	0.029	0.000		
FESI04	FE-SI (0.8,0.2)	2.53	2.82	0.028	0.001	0.025	-0.001
FESI05	FE-SI (0.75,0.25)	2.53	2.85	0.027	0.005		
FESI06	FE-SI (0.7,0.3)	2.63	3.00	0.033	0.002		
FEB01	FE-B (0.85,0.15)	3.10	3.64	0.033	-0.011		
FEB02	FE-B (0.8,0.2)	2.88	3.13	0.026	-0.009	0.025	-0.006
FEB03	FE-B (0.75,0.25)	2.51	2.79	0.024	-0.001		
FEB04	FE-B (0.5,0.5)	2.55	2.40	0.008	0.001		
FEB05	FE-B (0.85,0.15) (2)	2.98	3.48	0.032	-0.009		
FEB06	FE-B (0.85,0.15) (3)	3.05	3.56	0.033	-0.010		
FEB07	FE-B (0.85,0.15) (1)	2.99	3.47	0.031	-0.008		

TABLE III

CODE	SAMPLE	H_s (Oe)	ΔH_s (Oe)	$(4\pi M_s)$ (kG)	$(4\pi M_s')$ (kG)	$\lvert Q \rvert / M_s$ (10^{-6} G^{-1})
FE01	FE	27.5	23.0	20.6	8.6	20.1
NI01	NI	-	-	6.1	-	14.0
CO01	CO	41.0	23.0	16.8	2.5	20.1
NIFE06	NI-FE (0.75,0.25)	1.3	0.6	11.2	12.8	20.9
NIFE07	NI-FE (0.68,0.32)	3.6	3.4	13.7	14.4	19.3
NIFE02	NI-FE (0.8,0.2) 250A FE	5.7	3.8	13.9	14.7	32.0
NIFE03	NI-FE (0.8,0.2) 125A FE	1.4	1.2	11.4	12.5	39.8
NIFE04	NI-FE (0.68,0.32) 250A FE	3.8	3.8	19.6	20.6	32.3
NIFE08	NI-FE (0.68,0.32) 125A FE	16.2	19.0	11.5	8.3	32.4
NIFE09	NI-FE (0.75,0.25) 250A FE	10.0	15.3	15.5	15.0	32.1

TABLE IV

CODE	SAMPLE	H_s (Oe)	ΔH_s (Oe)	$(4\pi M_s)$ (kG)	$(4\pi M_s')$ (kG)	$\lvert Q \rvert / M_s$ ($10^{-6} G^{-1}$)
FESI01	FE-SI (0.9,0.1) (Easy)	30.0	13.4	19.2	14.0	15.0
FESI02	FE-SI (0.9,0.1) (Hard)	-	-	-	-	19.0
FESI03	FE-SI (0.85,0.15)	24.5	5.4	19.2	4.7	18.1
FESI04	FE-SI (0.8,0.2)	19.0	4.0	19.0	6.6	18.7
FESI05	FE-SI (0.75,0.25)	20.0	4.2	16.4	9.0	21.1
FESI06	FE-SI (0.7,0.3)	20.0	3.6	14.6	11.9	28.1
FEB01	FE-B (0.85,0.15)	1.9	1.0	18.2	18.4	23.6
FEB02	FE-B (0.8,0.2)	4.3	2.0	14.9	14.9	23.9
FEB03	FE-B (0.75,0.25)	2.0	10.3	17.0	17.0	17.7
FEB04	FE-B (0.5,0.5)	32.0	6.5	5.3	3.5	16.8
FEB05	FE-B (0.85,0.15) (2)	-	-	16.0	-	27.3
FEB06	FE-B (0.85,0.15) (3)	-	-	16.0	-	27.6
FEB07	FE-B (0.85,0.15) (1)	-	-	16.0	-	26.2

References

1. M.J. Freiser, "A Survey of Magneto-optic Effects." IEEE Trans. Magnetics MAG-4, 152 (1968).

2. W. Voigt, "Magneto-und Electrooptik", Teubner, Leipzig (1908).

3. P.N. Argyres, "Theory of Faraday and Kerr Effects in Ferromagnetics", Phys. Rev. 97, 334 (1955).

4. J.A. Copeland, C.K. Kuo, and E.J. Schneibner, Rev. Sci. Instr. 36, 291 (1965).

5. R.P. Hunt, "Magneto-Optic Scattering from Thin Solid Films", J. Appl. Phys. 38, 1652 (1967).

6. D.O. Smith, "Magneto-optical Scattering from Multilayer Magnetic and Dielectric Films", Part I. General Theory, Optica Acta 12, 13 (1965); Part II. Applications of the General Theory, Optica Acta 12, 193 (1965).

7. T. Yoshino and S. Tanaka, "Longitudinal Magneto-Optic-Effect in Ferromagnetic Thin Films". I. Japan J. Appl. Phys. 5, 989 (1966), II. (with T. Takahashi) Japan J. Appl. Phys. 5, 994 (1966).

8. J.H. Judy, J.K. Alstad, G. Bate, and J.R. Wiitala, "Large Longitudinal Kerr Rotations and Figures of Merit for Thin Iron Films", IEEE Trans. Magnetics MAG-4, 401 (1968).

9. R.M. Bozorth, "Ferromagnetism", Van Nostrand, New York (1951).

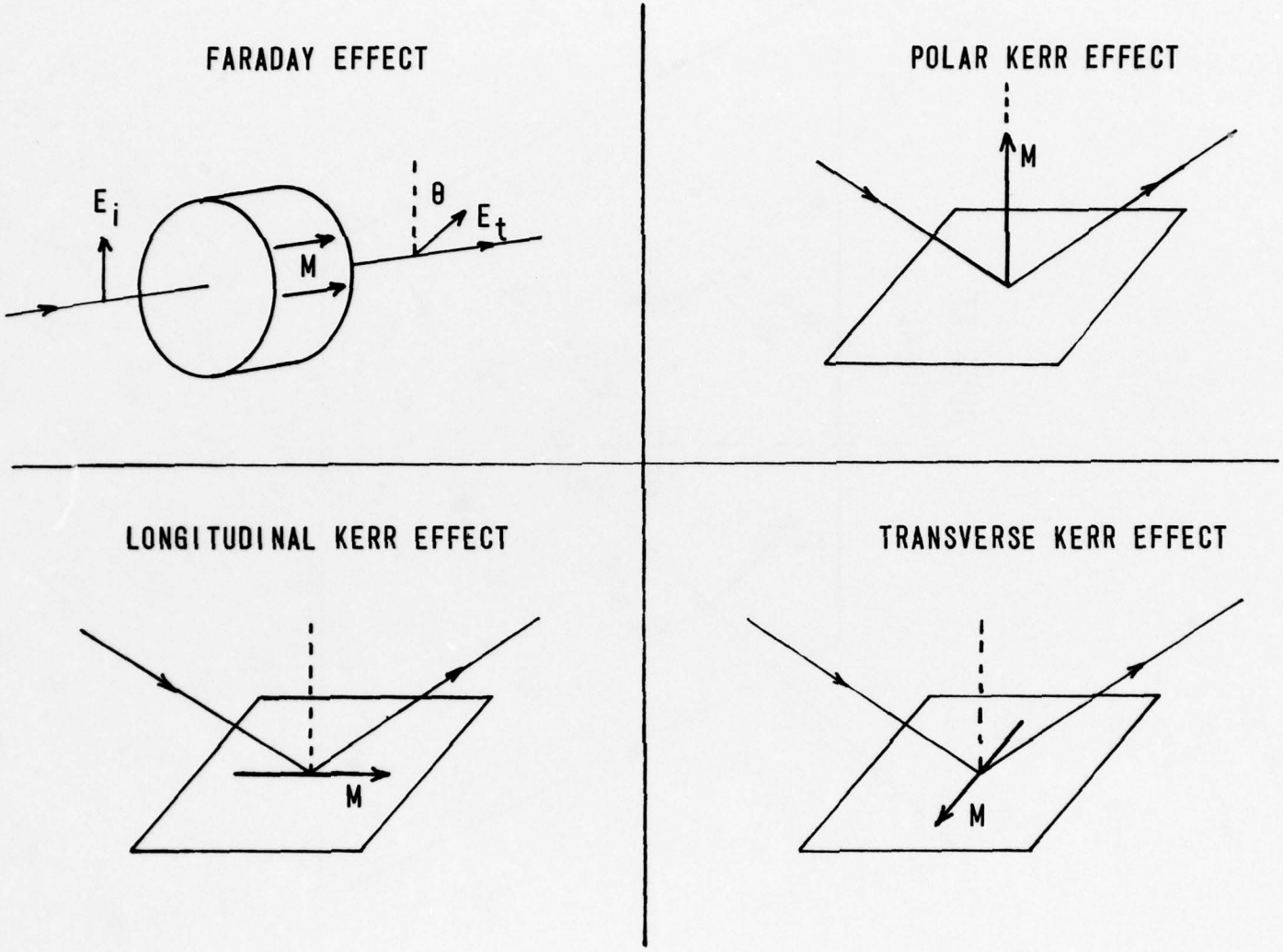
FARADAY EFFECT
E_i
M
θ
E_t
POLAR KERR EFFECT
M
LONGITUDINAL KERR EFFECT
M
TRANSVERSE KERR EFFECT
M

Figure 1

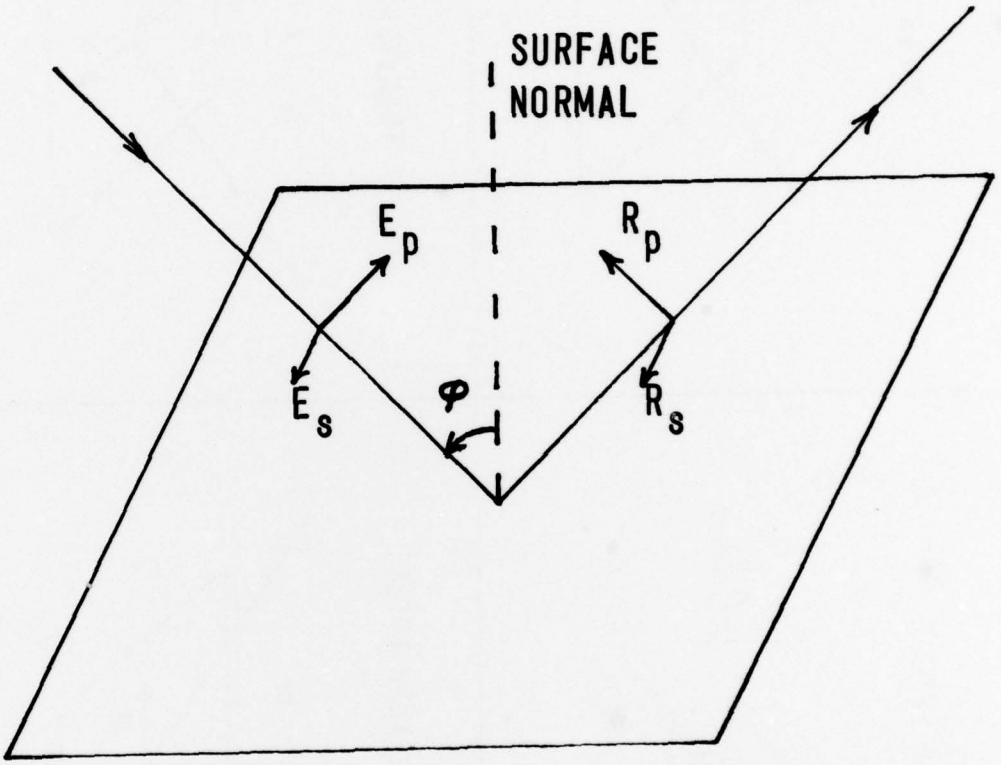

Figure 2

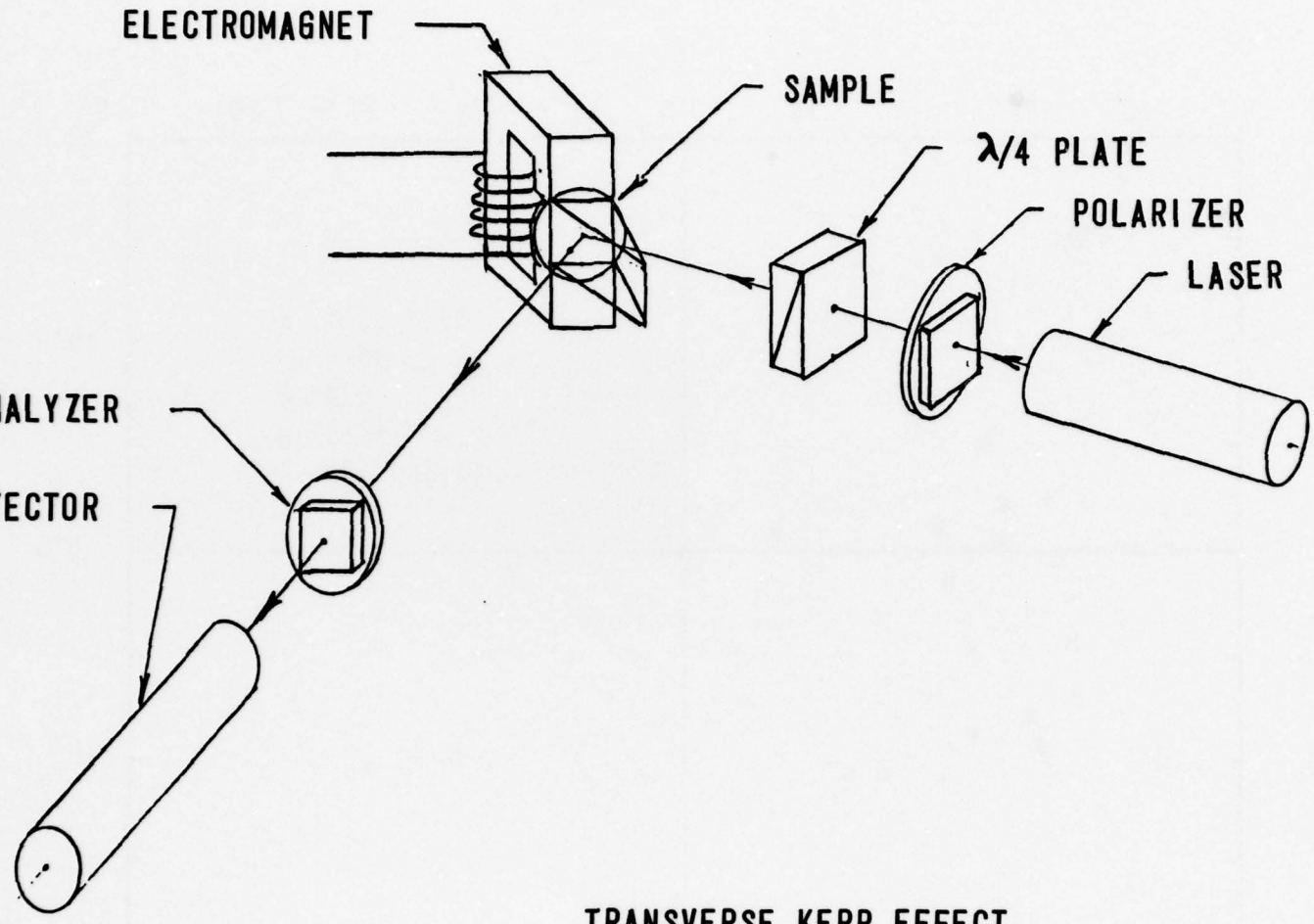

TRANSVERSE KERR EFFECT

Figure 3

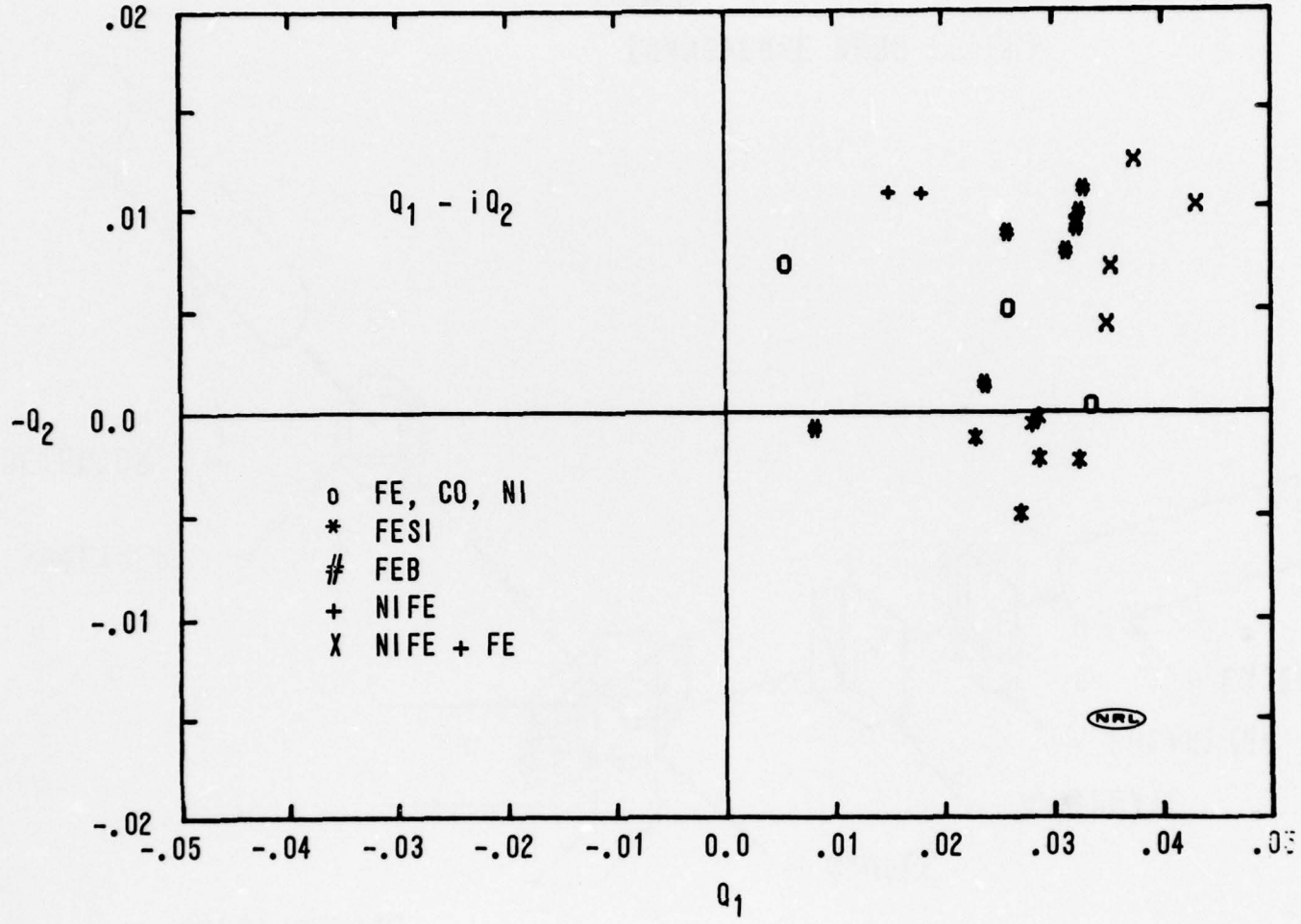
.02
.01
0.0
-.01
-.02
$-Q_2$
$Q_1 - iQ_2$
o FE, CO, NI
* FESI
# FEB
+ NIFE
X NIFE + FE
NRL
-.05
-.04
-.03
-.02
-.01
0.0
.01
.02
.03
.04
Q_1

Figure 4

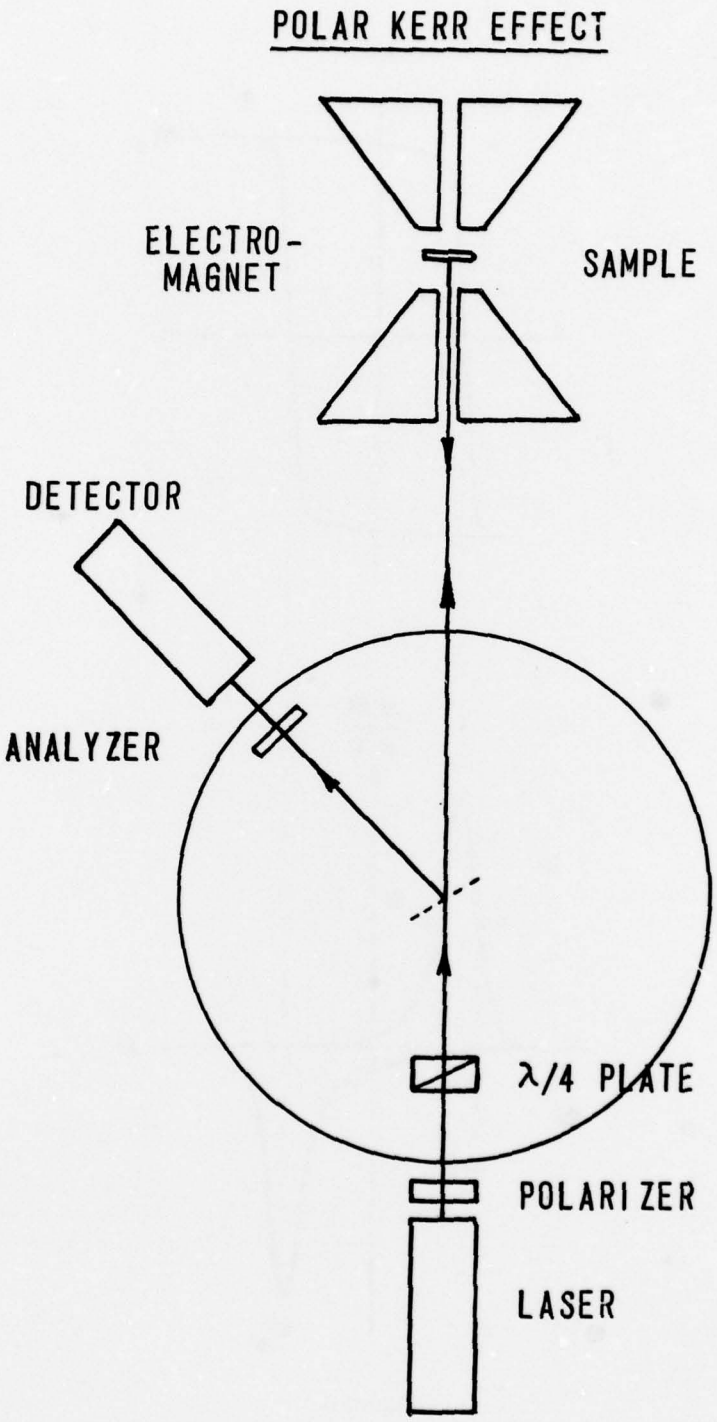
POLAR KERR EFFECT
ELECTRO-
MAGNET
SAMPLE
DETECTOR
ANALYZER
λ/4 PLATE
POLARIZER
LASER

Figure 5

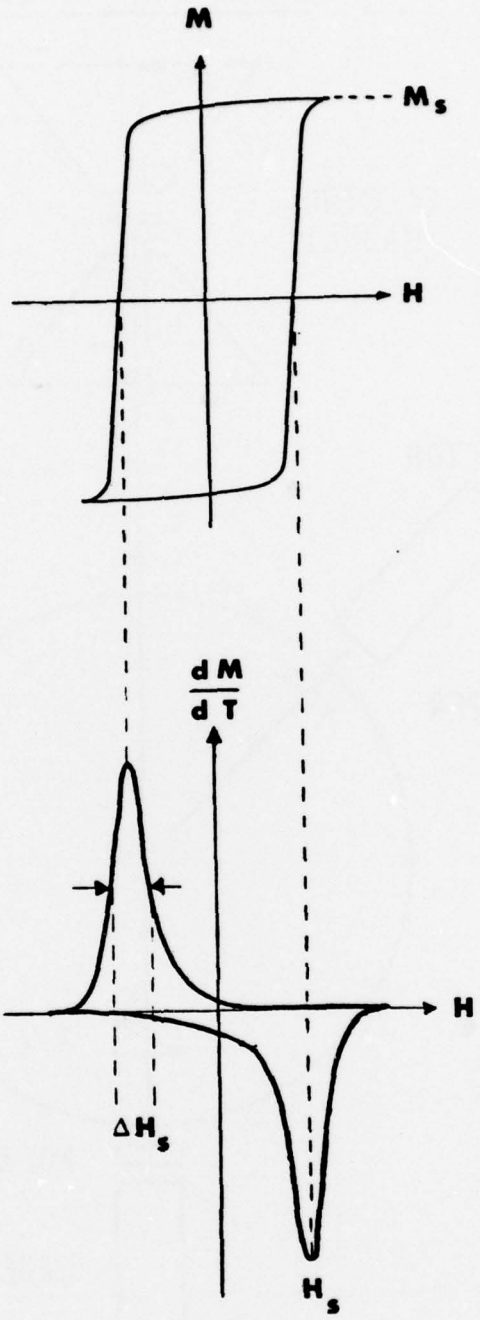

Figure 6

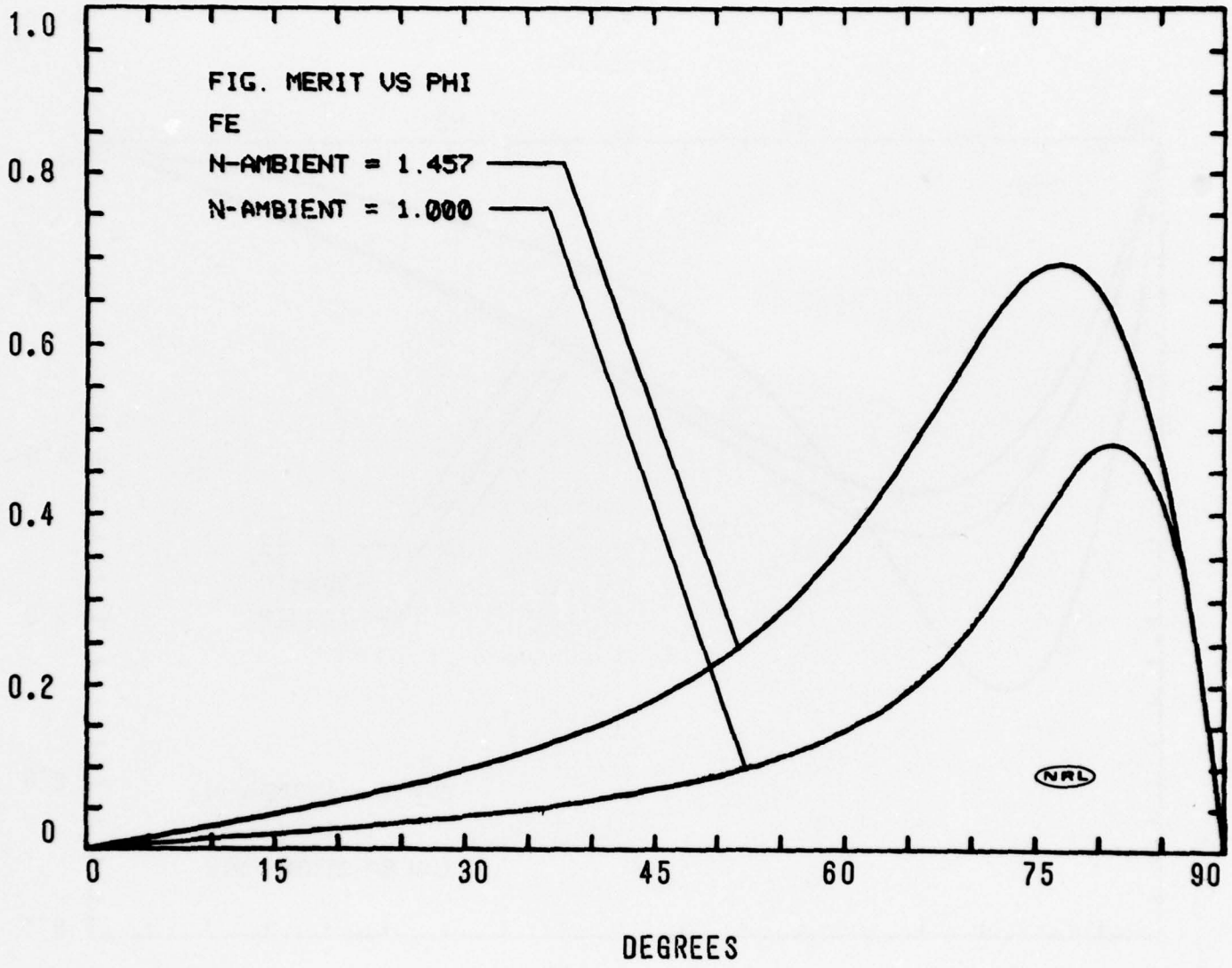
FIG. MERIT VS PHI
FE
N-AMBIENT = 1.457
N-AMBIENT = 1.000
1.0
0.8
0.6
0.4
0.2
0
0
15
30
45
60
75
90
DEGREES
NRL

Figure 7

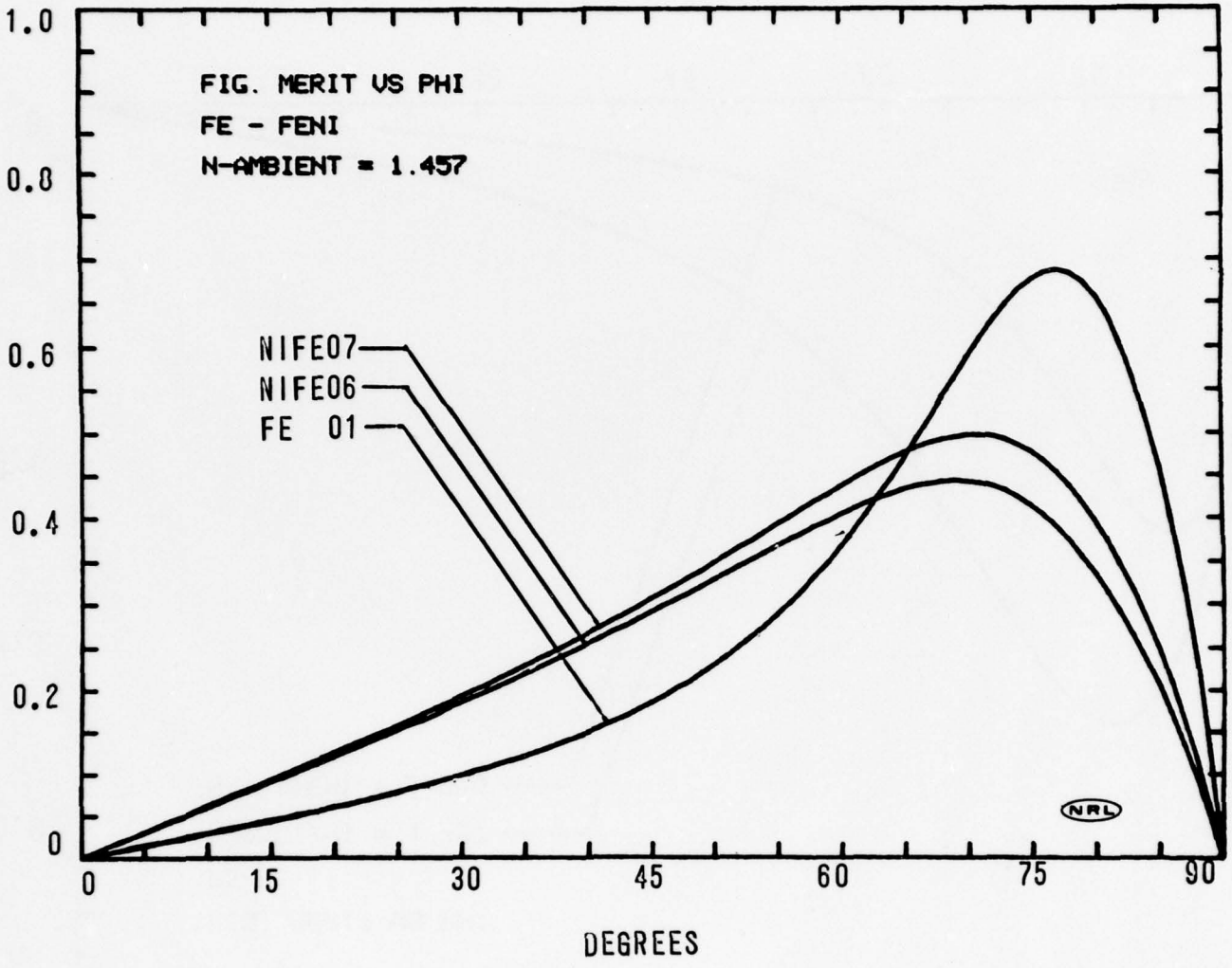
FIG. MERIT VS PHI
FE - FENI
N-AMBIENT = 1.457
NIFE07
NIFE06
FE 01
NRL
1.0
0.8
0.6
0.4
0.2
0
0
15
30
45
60
75
90
DEGREES

Figure 8

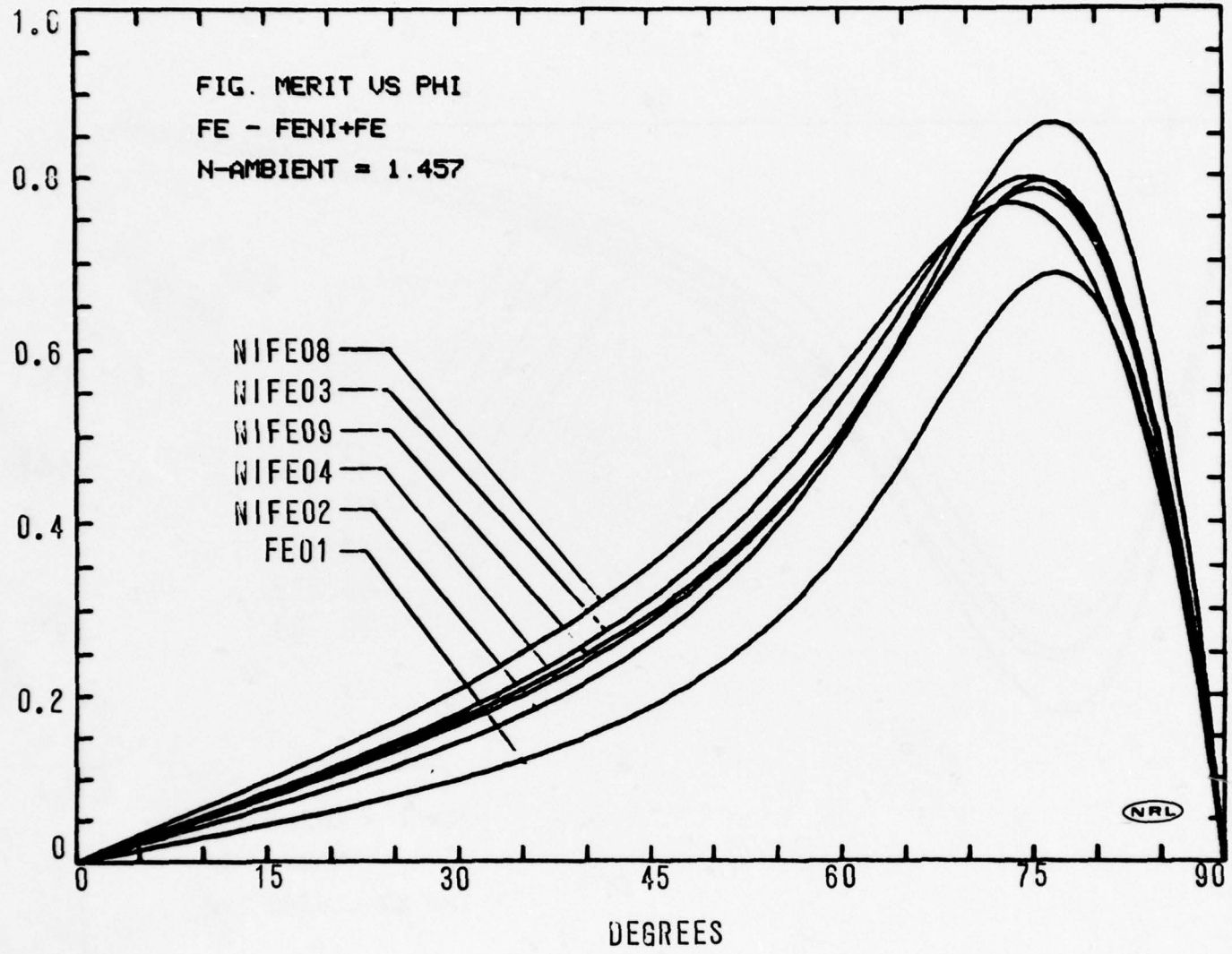
FIG. MERIT VS PHI
FE - FENI+FE
N-AMBIENT = 1.457
NIFE08
NIFE03
NIFE09
NIFE04
NIFE02
FE01
1.0
0.8
0.6
0.4
0.2
0
0
15
30
45
60
75
90
DEGREES
NRL

Figure 9

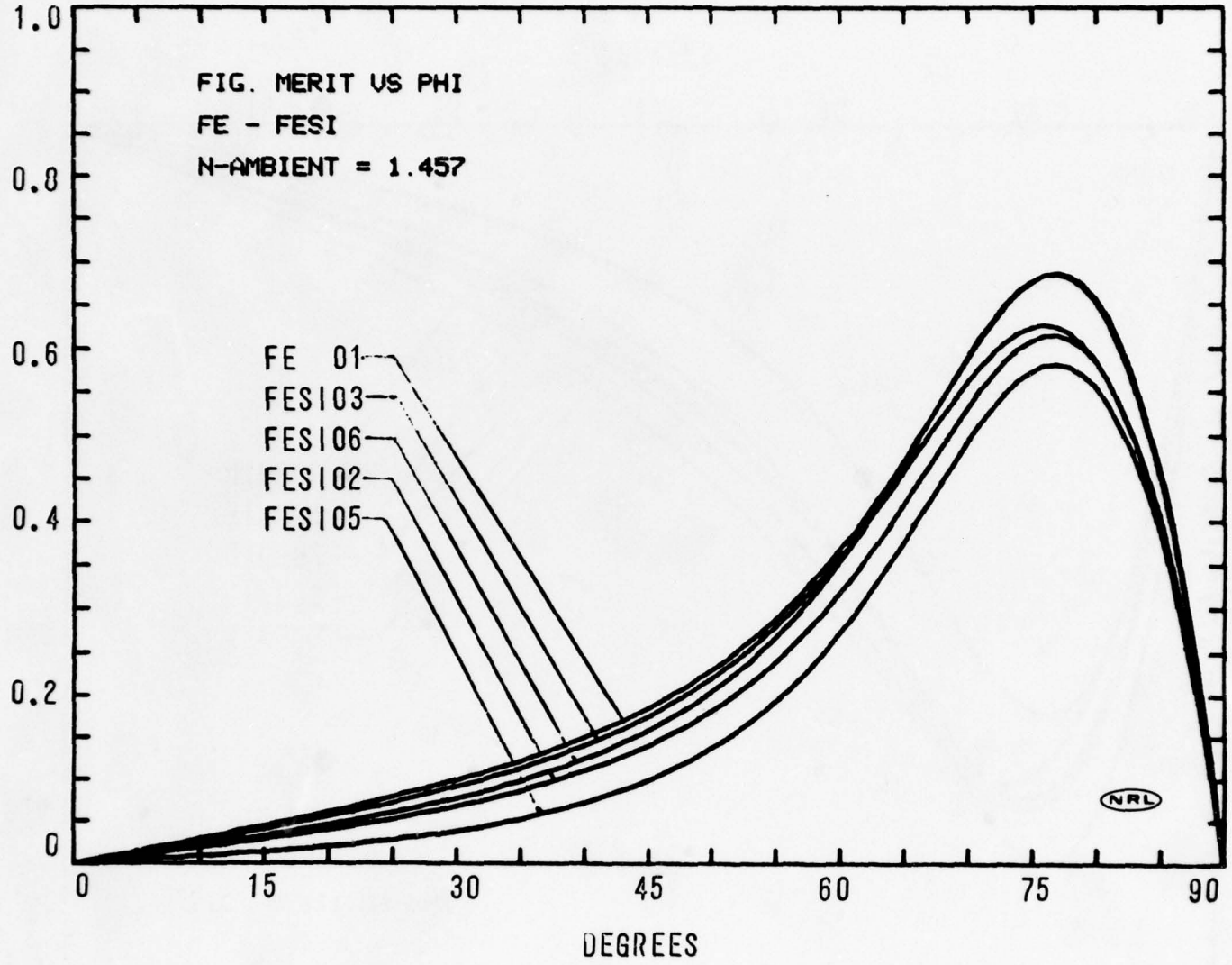
FIG. MERIT VS PHI
FE - FESI
N-AMBIENT = 1.457
FE 01
FESI03
FESI06
FESI02
FESI05
1.0
0.8
0.6
0.4
0.2
0
0
15
30
45
60
75
90
DEGREES
NRL

Figure 10

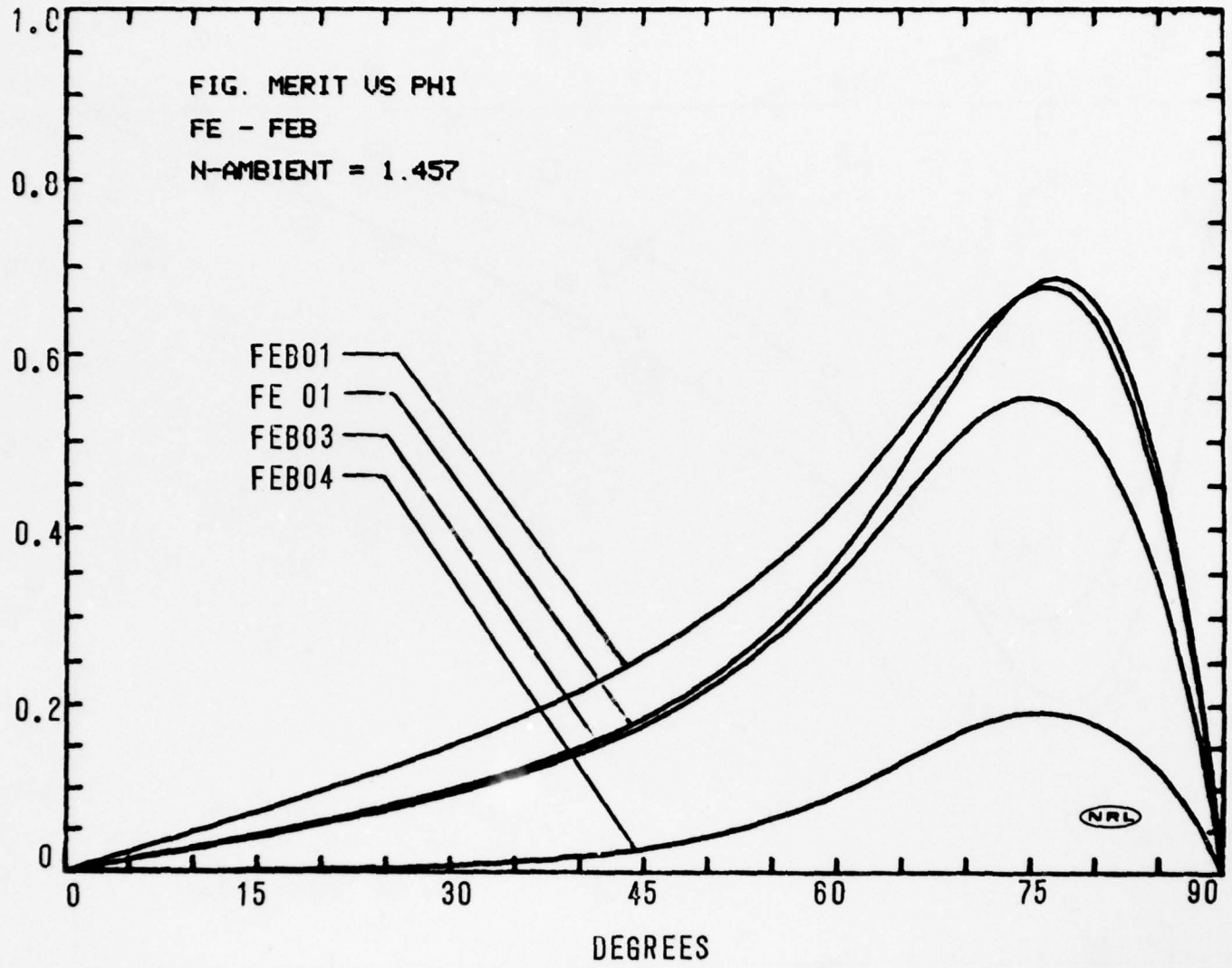
FIG. MERIT VS PHI
FE - FEB
N-AMBIENT = 1.457
FEB01
FE 01
FEB03
FEB04
NRL
1.0
0.8
0.6
0.4
0.2
0
0
15
30
45
60
75
90
DEGREES

Figure 11

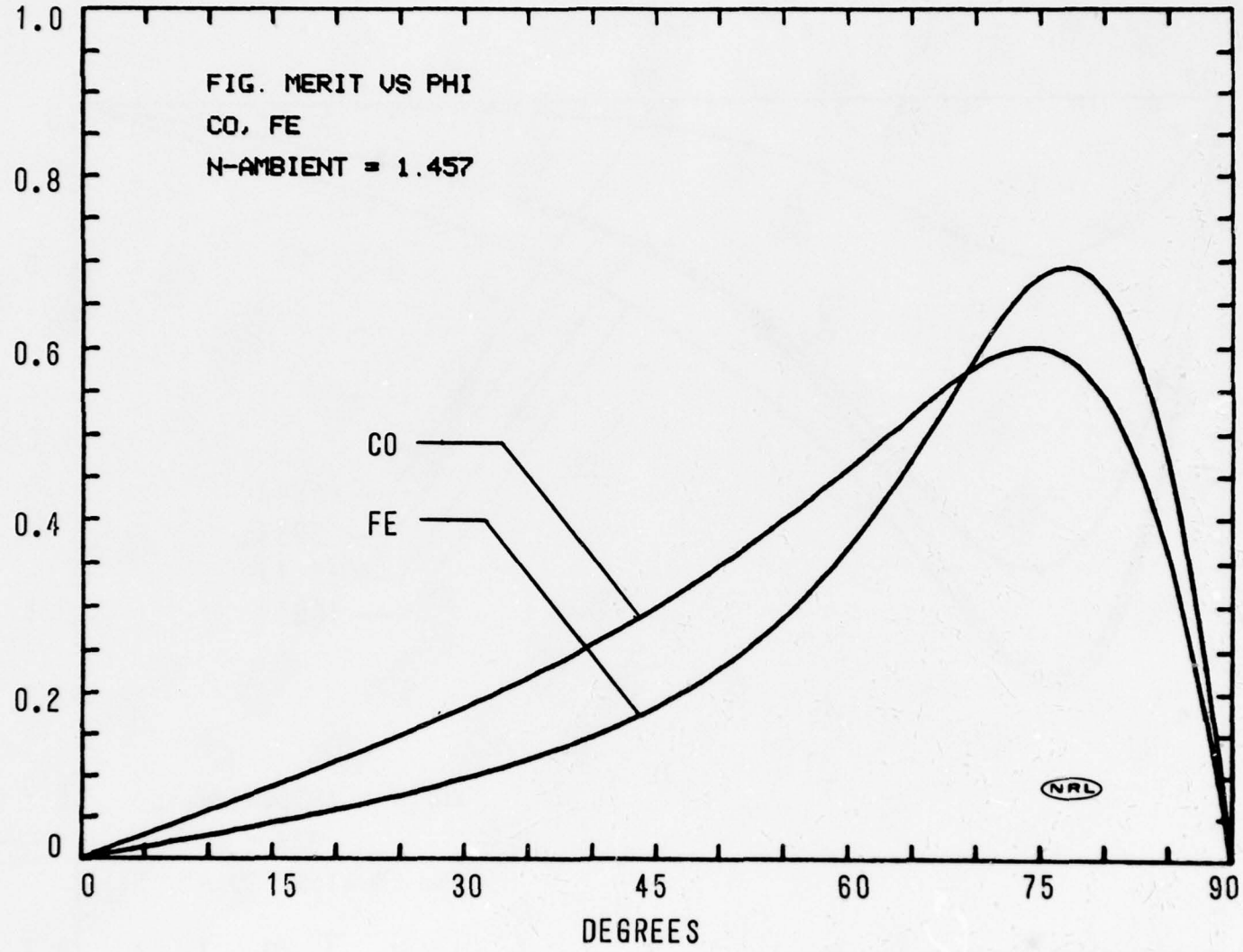
FIG. MERIT VS PHI
CO, FE
N-AMBIENT = 1.457
CO
FE
NRL
1.0
0.8
0.6
0.4
0.2
0
0
15
30
45
60
75
90
DEGREES

Figure 12

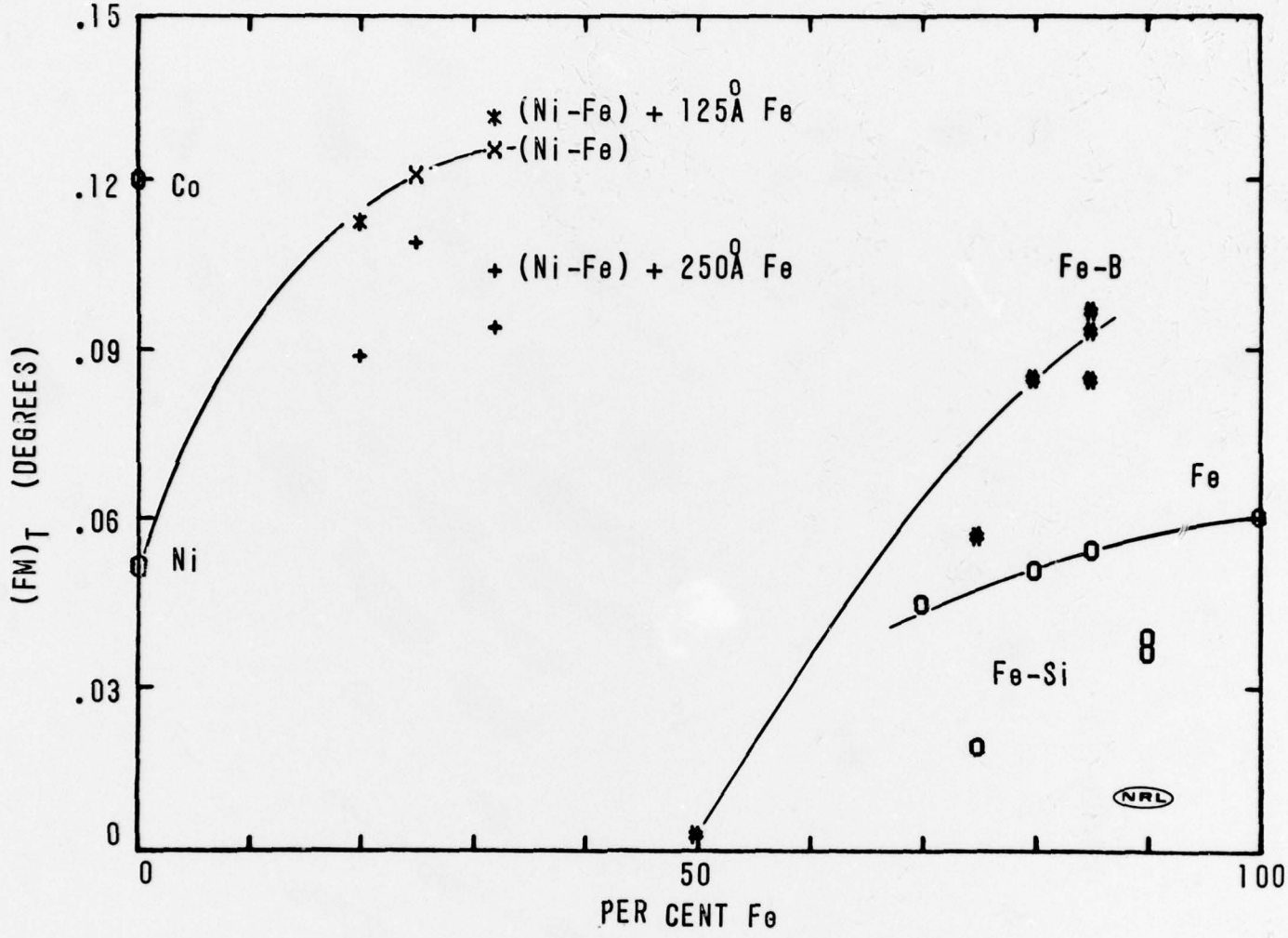
.15
.12
.09
.06
.03
0
(FM)T (DEGREES)
* (Ni-Fe) + 125Å Fe
×-(Ni-Fe)
+ (Ni-Fe) + 250Å Fe
Co
Ni
Fe-B
Fe
Fe-Si
8
NRL
0
50
100
PER CENT Fe

Figure 13